Supporting Information

Coumarin-based emissive hexacatenars: synthesis, 2D, 3D self-assembly and photodimerization

Yulong Xiao,‡[a] Xiaoping Tan,‡[b, a] Wei Xing,[a] Kai Zhao,[a] Bei Zhang,[a] and Xiaohong Cheng*[a]

[a] Key Laboratory of Medicinal Chemistry for Natural Resources, Chemistry Department, Yunnan University
Kunming,
Yunnan 650091,
P. R. China
Fax: (+86) 871 65032905
E-mail: xhcheng@ynu.edu.cn

[b] School of Chemistry and Chemical Engineering, Yangtze Normal University, Chongqing, 408100, China

‡Both authors contributed equally to this work

Content

1 Additional Experimental Data

1.1 Experimental techniques

A Mettler heating stage (FP 82 HT) was used for polarizing optical microscopy (POM, Optiphot 2, Nikon) and DSC were recorded with a DSC 200 F3 Maia calorimeter (NETZSCH) at 5 K min^{-1}.

SEM experiments were carried out on a QUNT200 scanning electron microscopy (SEM, USA). All pictures were taken digitally. For the sample preparation, the gel was placed on an aluminium foil for some time until the gel became dry gel, then the sample was gold plated, finally the sample was put the sample into the scanning electron microscopy for observation. XRD measurement of xerogels was used the X-ray powder diffraction (XRD, Rigaku Co., Tokyo, Japan) analysis was conducted on a D/max-3B spectrometer with Cu Kα radiation.

Small-angle powder diffraction (SAXS) experiments were performed in transmission mode with synchrotron radiation at the 1W2A SAXS beamline at Beijing Accelerator Laboratory.[S1] A modified Linkam hot stage with a thermal stability within 0.2 °C was used, with a hole for the capillary drilled through the silver heating block and mica windows attached to it on each side. Samples were held in the poly(imide) (Kapton) film. A MarCCD 165 detector was used. q calibration and linearization were verified using several orders of layer reflections from silver behemate. Positions and intensities of the diffraction peaks were measured using PeakSolve™ (Galactic).

Electron density reconstruction. Fourier reconstruction of the electron density was carried out using the general formula for 2D periodic systems:

$$E(xy) = \Sigma_{hk} \text{ sqrt}[I(hk)] \exp[i2\pi(hx+ky) + \phi_{hk}]$$

here m being the multiplicity, F the structure factor, which is proportional to the intensity and φ the phase of the reflex.

1.2 Molecular dynamics simulation

Annealing dynamics runs were carried out using the Universal Force Field (Material Studio, Accelrys). The structure in Fig.1e was obtained with 2 molecules in a square prism box with the side equal to the unit cell length and a height of 0.45nm, with 3d periodic boundary conditions. 30 temperature cycles of NVT dynamics were run between 300 and 500 K, with a total annealing time of 30 ps.

Annealing dynamics runs were carried out using the Universal Force Field (Material Studio, Accelrys). The structure in Fig.1f and 4d were obtained with 2 molecules and 1 molecule respectively in a 60 degree rhombic prism box with the side equal to the unit cell length and a

height of 0.45 nm, with 3D periodic boundary conditions. 30 temperature cycles of NVT dynamics were run between 300 and 500 K, with a total annealing time of 30 ps.

Annealing dynamics runs were carried out using the Universal Force Field (Material Studio, Accelrys). The structure in Fig.2b was obtained with 2 molecules in a rectangular box with the side equal to the lattice parameters and a height of 0.45 nm, with 3d periodic boundary conditions. 30 temperature cycles of NVT dynamics were run between 300 and 500 K, with a total annealing time of 30 ps.

1.2 Additional textures of LC phases and DSC traces

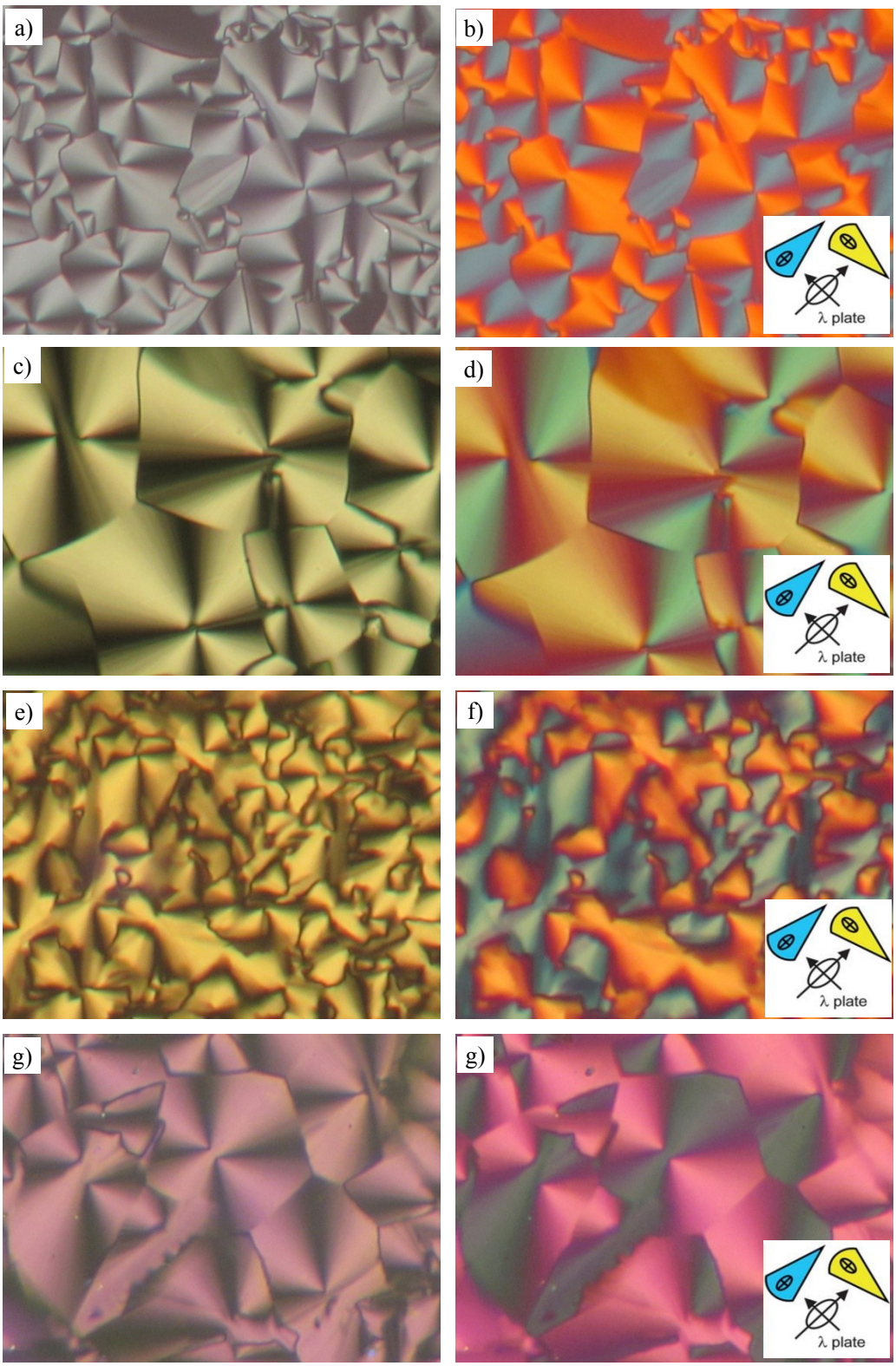

Fig. S1 Representative textures between crossed polarizers: (a) the texture of Col_{squ}/*p*4*mm* phase of **C/10** cooling at 80 °C; (b) the same texture with λ-retarder plate (the indicatrix orientation in the compensator is shown on the right; the columnar phase is optically negative as indicated by the orientation of the blue shifted and yellow shifted fans; this means that in the columns the preferred direction of the intramolecular π-conjugation pathway - coinciding with the long axis of the aromatic cores is on average perpendicular to the column long axis; (c) the texture of Col_{hex}/*p*6*mm* phase of **C/12** cooling at 90 °C; (d) the same texture with λ-retarder plate; (e) the texture of

$Col_{rec}/p2mm$ phase of **C/16** cooling at 80 °C; (f) the same texture with λ-retarder plate; (g) the texture of $Col_{hex}/p6mm$ phase of **C/18** cooling at 80 °C; (d) the same texture with λ-retarder plate.

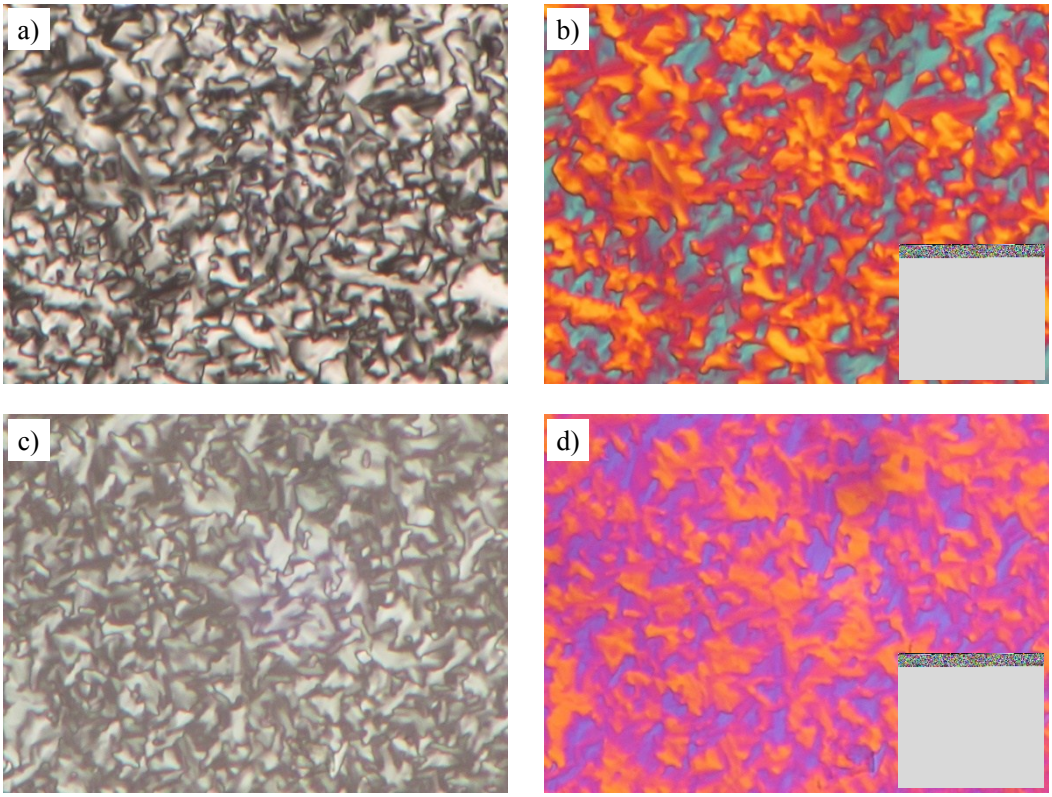

Fig. S2 Representative textures between crossed polarizers: (a) the texture of $Col_{hex}/p6mm$ phase of photodimer **IC/10** cooling at 80 °C; (b) the same texture with λ-retarder plate (the indicatrix orientation in the compensator is shown on the right; the columnar phase is optically negative as indicated by the orientation of the blue shifted and yellow shifted fans; this means that in the columns the preferred direction of the intramolecular π-conjugation pathway - coinciding with the long axis of the aromatic cores is on average perpendicular to the column long axis; (c) the texture of $Col_{hex}/p6mm$ phase of photodimer **IC/12** cooling at 90 °C; (d) the same texture with λ-retarder plate.

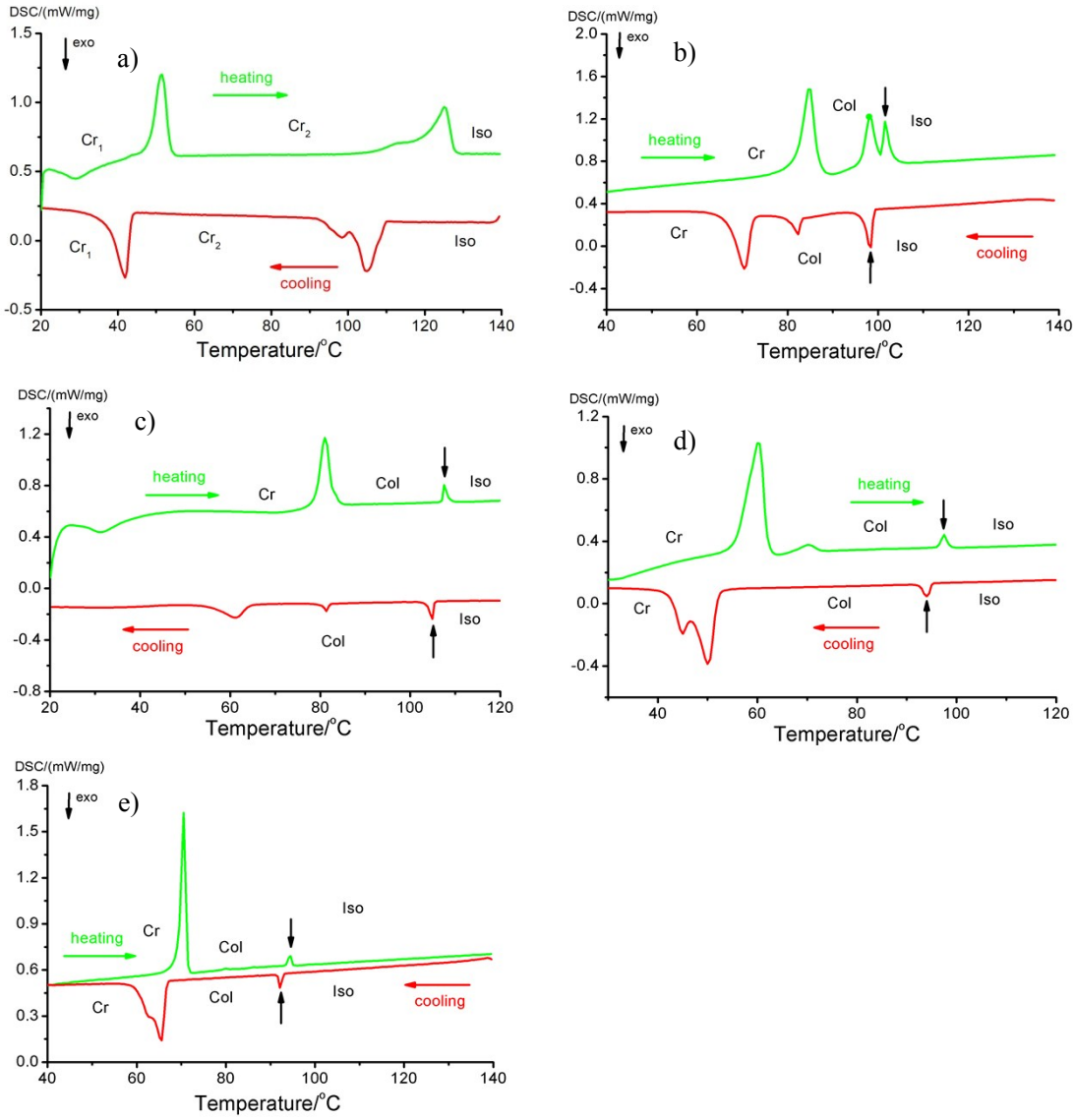

Fig. S3 DSC heating and cooling scans (5 K min^{-1}) of (a) compound **C/8** (first scans); (b) compound **C/10** (first scans); (second scans); (c) compound **C/12** (first scans); (d) compound **C/16** (first scans); (e) compound **C/18** (first scans).

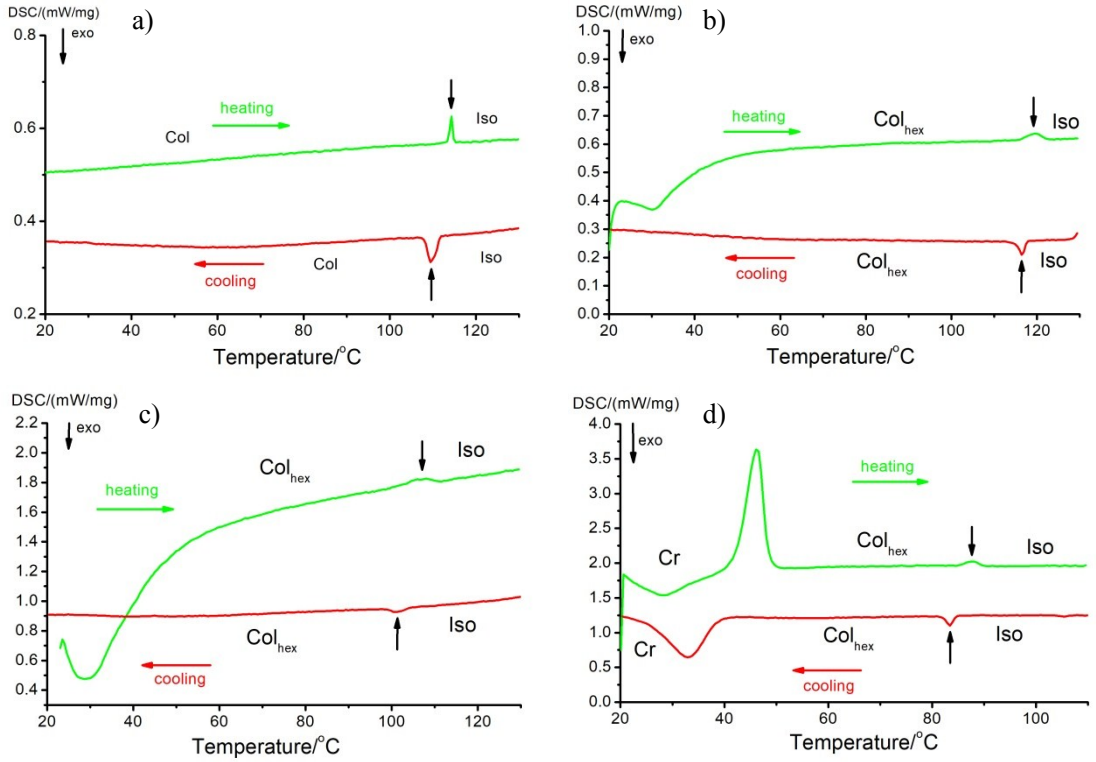

Fig. S4 DSC heating and cooling scans (5 K min^{-1}) of (a) compound photodimer **ICT/8** (first scans); (b) compound photodimer **ICT/10** (second scans); (c) compound photodimer **ICT/12** (first scans); (d) compound photodimers **ICT/16** (first scans).

1.3 Additional XRD data

Table S1 Experimental and calculated *d*-spacings of the observed SAXS reflections of the square phase in compound **C/10** at 90 °C. All intensity values are Lorentz and multiplicity corrected.

(*hk*)	$d_{obs.}$ – spacing (nm)	$d_{cal.}$ – spacing (nm)	*intensity*	*phase*
(10)	3.58	3.58	100	-
(11)	2.54	2.54	10.2	-
(20)	1.80	1.80	2.2	-
a_{squ}= 3.59 nm				

Table S2 Experimental and calculated *d*-spacings of the observed SAXS reflections of the hexagonal phase in compound **C/10** at 100 °C. All intensity values are Lorentz and multiplicity corrected.

(*hk*)	$d_{obs.}$ – spacing (nm)	$d_{cal.}$ – spacing (nm)	*intensity*	*phase*
(10)	3.63	3.63	100	0
(11)	2.11	2.11	3.2	0
(20)	1.82	1.82	2.5	-

a_{hex}= 3.64 nm

Table S3 Experimental and calculated *d*-spacings of the observed SAXS reflections of the rectangular phase in compound **C/12** at 80 °C. All intensity values are Lorentz and multiplicity corrected.

(*hk*)	$d_{obs.}$ – spacing (nm)	$d_{cal.}$ – spacing (nm)	*intensity*	*phase*
(10)	4.41	4.41	100	-
(01)	3.46	3.46	56.3	-
(20)	2.22	2.21	6.3	-
a = 4.41 nm, b = 3.46 nm				

Table S4 Experimental and calculated *d*-spacings of the observed SAXS reflections of the hexagonal phase in compound **C/12** at 100 °C. All intensity values are Lorentz and multiplicity corrected.

(*hk*)	$d_{obs.}$ – spacing (nm)	$d_{cal.}$ – spacing (nm)	*intensity*	*phase*
(10)	3.57	3.57	100	0
(11)	2.08	2.08	3.4	0
(20)	1.80	1.80	1.0	-
a_{hex}= 3.59 nm				

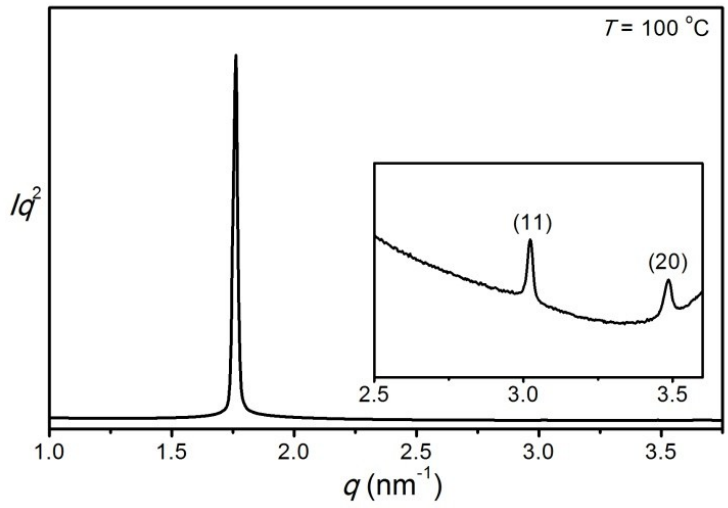

Fig. S5 SAXS diffraction pattern of hexagonal phase of compound **C/12** recorded at 100 °C.

Table S5 Experimental and calculated *d*-spacings of the observed SAXS reflections of the rectangular phase in compound **C/16** at 100 °C. All intensity values are Lorentz and multiplicity corrected.

(*hk*)	$d_{obs.}$ – spacing (nm)	$d_{cal.}$ – spacing (nm)	*intensity*	*phase*
(10)	4.36	4.36	54.2	0
(01)	3.85	3.85	100	0
(20)	2.18	2.18	3.2	-
a = 4.36 nm, b = 3.85 nm				

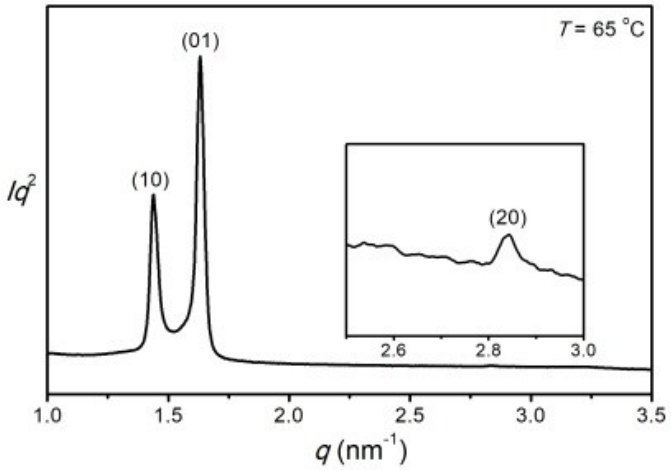

Fig. S6 SAXS diffraction pattern of rectangular phase of compound **C/16** recorded at 65 °C.

Table S6 Experimental and calculated *d*-spacings of the observed SAXS reflections of the hexagonal phase in compound **C/18** at 100 °C. All intensity values are Lorentz and multiplicity corrected.

(*hk*)	$d_{obs.}$ – spacing (nm)	$d_{cal.}$ – spacing (nm)	*intensity*	*phase*
(10)	4.13	4.13	100	0
(11)	2.39	2.39	0.6	0
(20)	2.06	2.06	1.4	-
a_{hex}= 4.14 nm				

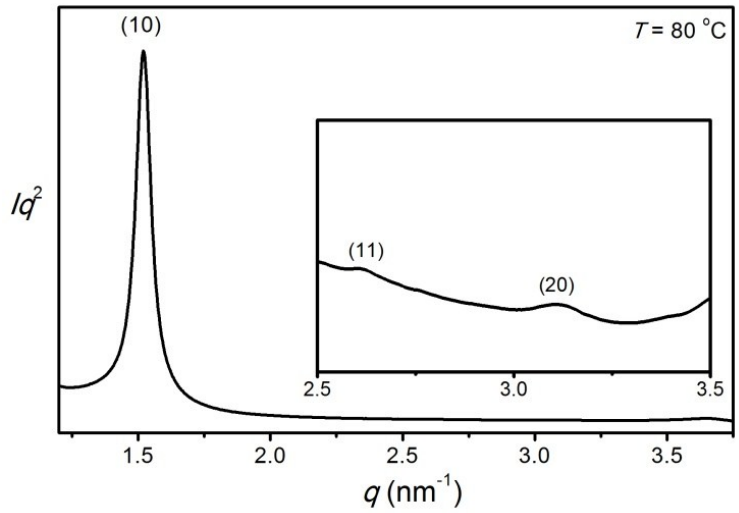

Fig. S7 SAXS diffraction pattern of hexagonal phase of compound **C/18** recorded at 80 °C.

Table S7 Experimental and calculated *d*-spacings of the observed SAXS reflections of the hexagonal phase in photodimer **IC/8** at 25 °C. All intensity values are Lorentz and multiplicity corrected.

(*hk*)	$d_{obs.}$ – spacing (nm)	$d_{cal.}$–spacing (nm)	*intensity*	*phase*
(10)	3.17	3.17	100	-
(11)	1.75	1.82	0.6	-
(20)	1.60	1.59	0.8	-
a_{hex}= 3.62 nm				

Table S8 Experimental and calculated *d*-spacings of the observed SAXS reflections of the hexagonal phase in photodimer **IC/10** at 25 °C. All intensity values are Lorentz and multiplicity corrected.

(*hk*)	$d_{obs.}$ – spacing (nm)	$d_{cal.}$-spacing (nm)	*intensity*	*phase*
(10)	3.38	3.38	100	-
(11)	1.95	1.95	1.0	-
(20)	1.69	1.69	0.6	-
a_{hex}= 3.90 nm				

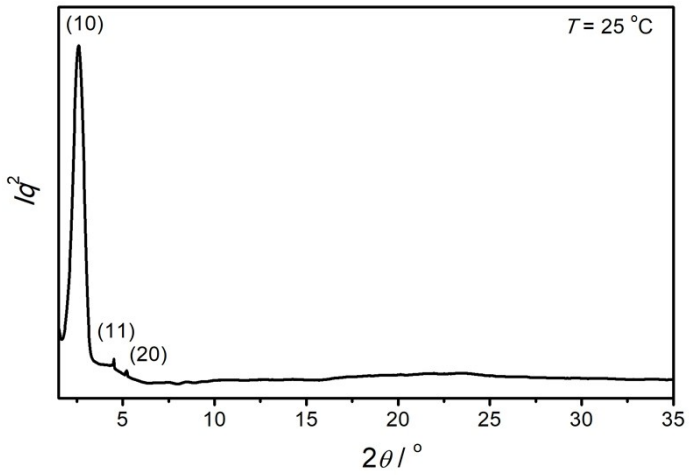

Fig. S8 SAXS diffraction pattern of hexagonal phase of photodimer **IC/10** recorded at 25 °C.

Table S9 Experimental and calculated *d*-spacings of the observed SAXS reflections of the hexagonal phase in photodimer **IC/12** at 25 °C. All intensity values are Lorentz and multiplicity corrected.

(*hk*)	$d_{obs.}$ – spacing (nm)	$d_{cal.}$ – spacing (nm)	*intensity*	*phase*
(10)	3.65	3.65	100	-
(11)	2.11	2.11	0.1	-
(20)	1.83	1.83	0.3	-
a_{hex}= 4.22 nm				

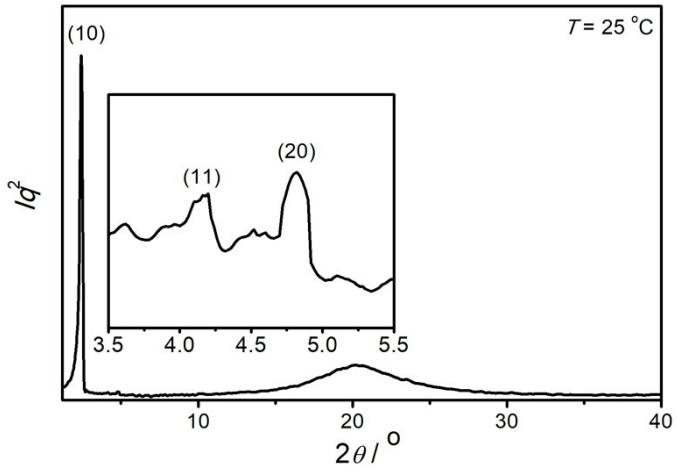

Fig. S9 SAXS diffraction pattern of hexagonal phase of photodimer **IC/12** recorded at 25 °C.

Table S10 Experimental and calculated *d*-spacings of the observed SAXS reflections of the hexagonal phase in photodimer **IC/16** at 65 °C. All intensity values are Lorentz and multiplicity corrected.

(*hk*)	$d_{obs.}$ – spacing (nm)	$d_{cal.}$ – spacing (nm)	*intensity*	*phase*

(10)	3.91	3.91	100	-
(11)	2.26	2.25	0.1	-
(20)	1.96	1.96	0.3	-
a_{hex}= 4.51 nm				

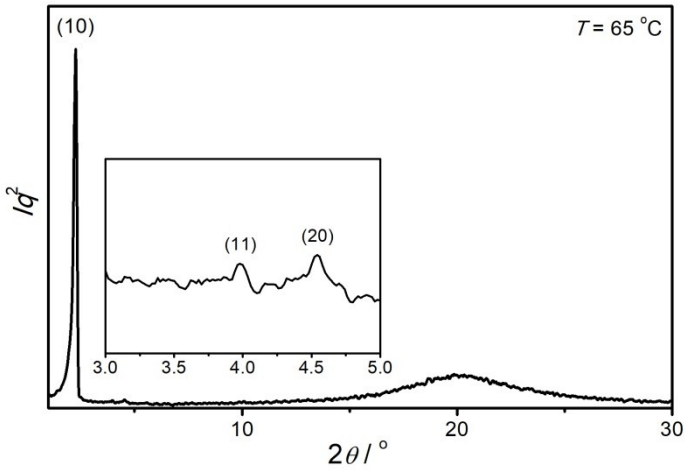

Fig. S10 (a) SAXS diffraction pattern of hexagonal phase of photodimer **IC/16** recorded at 65 °C.

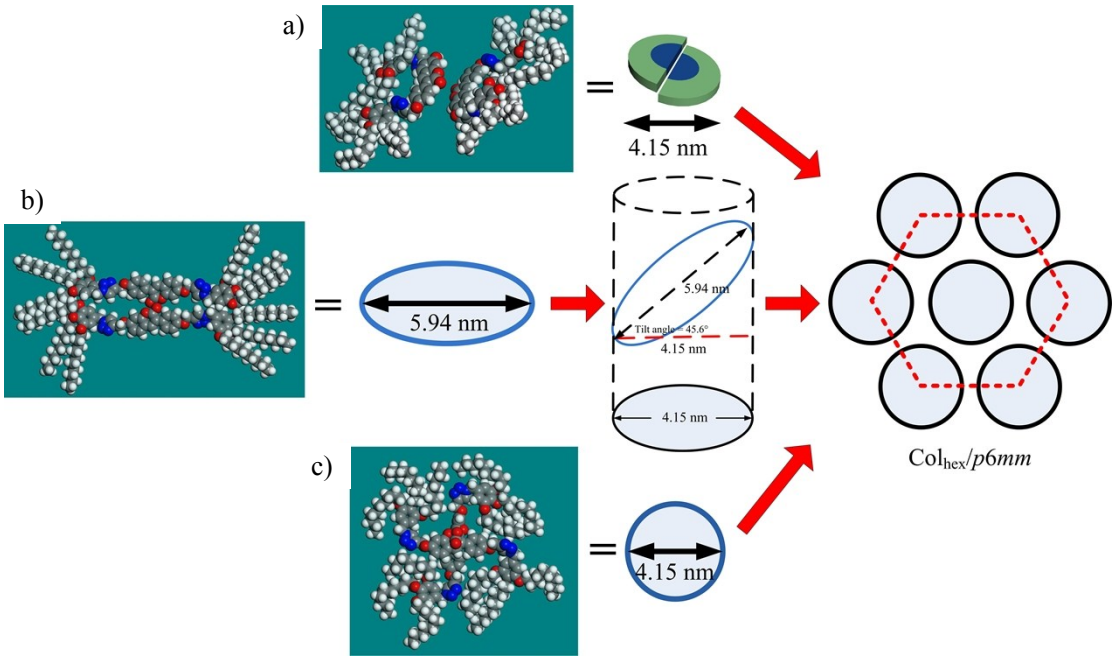

Fig. S11 Other possible self-assembly models of hexagonal columnar phase. (a) The molecules with bent-shape conformations are partially slipped antiparallel π-face-to-face packing due to the large dipole of the coumarin core (calculated to be 5.19 D), these antiparallel π-face-to-face dimer stacked into columns and finally formed hexagonal columnar phase; (b) The fully extended molecular shape of **C/10** is anisotropic with an elliptical core. The molecular length along the long axis was calculated to be 5.94 nm which is much longer than any of the intercolumnar distances in the hexagonal columnar phase, therefore the elliptical-shaped **C/10** molecules are arranged in a tilted fashion within columns; (c) Two molecules with bent-shape conformation are arranged in cross to form a disk and the diameter of the disk is equal to the lattice parameter of the hexagonal columnar phase. These

disks stacked into columns and finally formed hexagonal columnar phase.

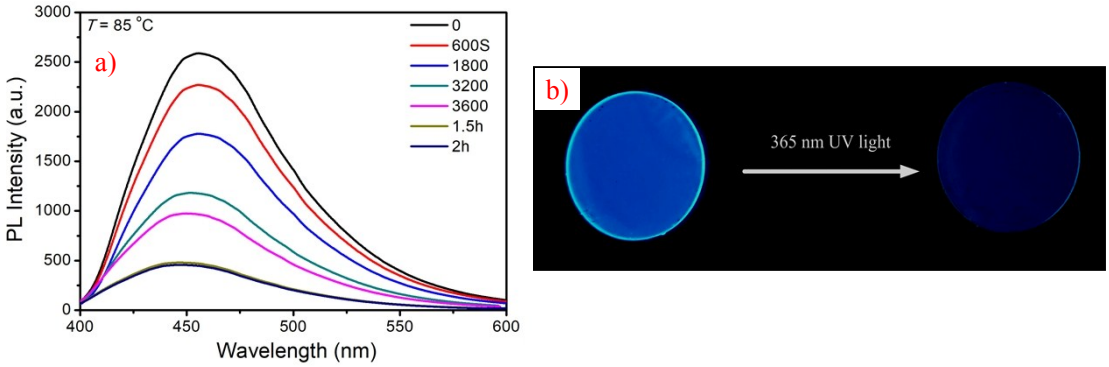

Fig. S12 (a) Fluorescence spectra of compound **C/10** in LC state upon 365 nm UV light irradiation with increasing time; (b) Fluorescence images of **C/10** in LC state before/after irradiated upon 365 nm UV light for 2 h.

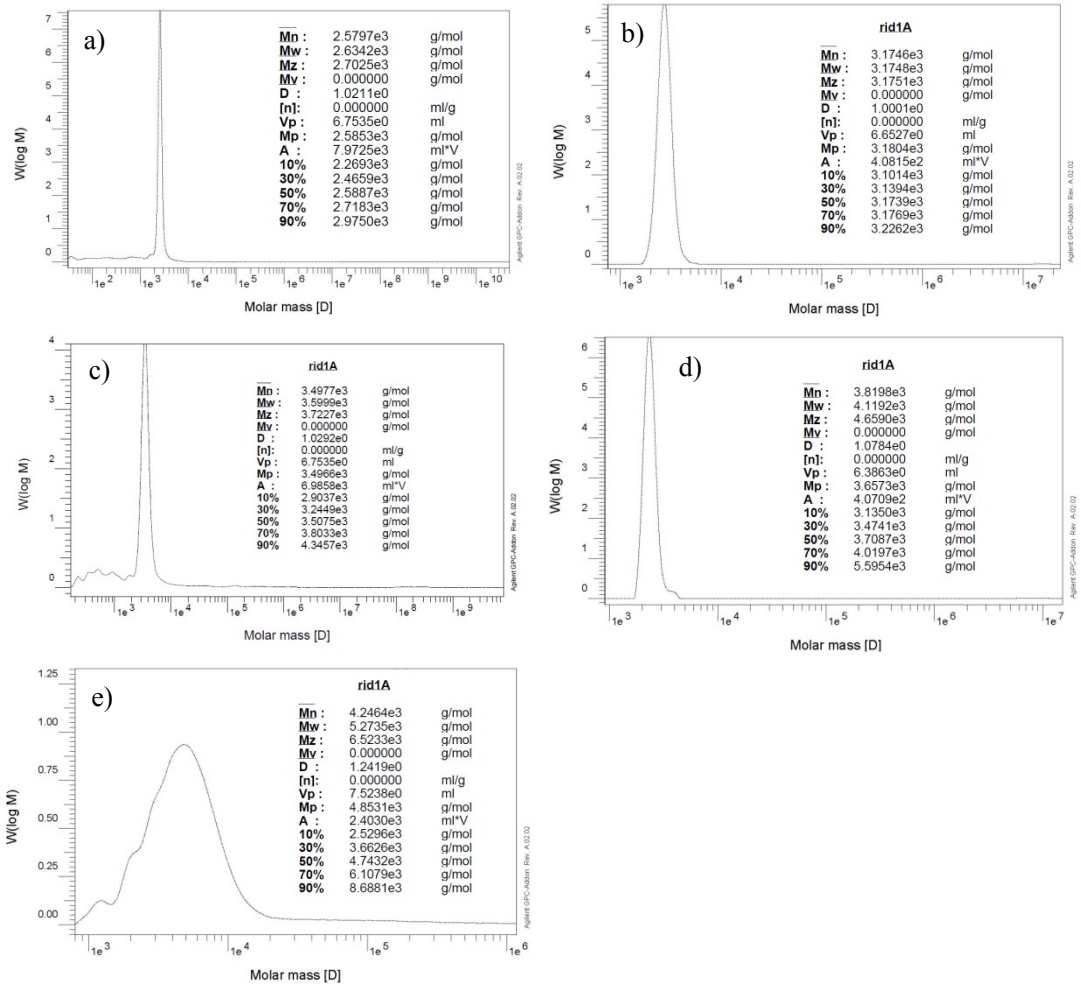

Fig. S13 The Gel Permeation Chromatography (GPC) of (a) photodimer **IC/8**; (b) photodimer **IC/10**; (c) photodimer **IC/12**; (d) photodimer **IC/16**; (e) photodimer **IC/18**.

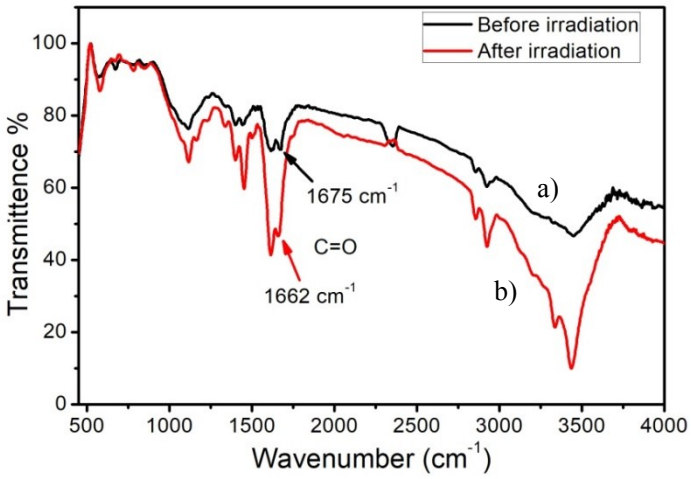

Fig. S14 The FT-IR spectrum of **C/10 (**a) before 365 nm UV irradiation; (b) after 365 nm UV irradiation.

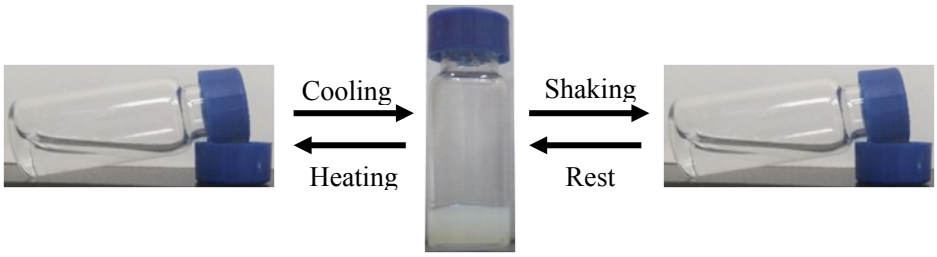

Fig. S15 Multistimuli responsive organogels of compound **C/10** in acetone (6.0 mg/mL).

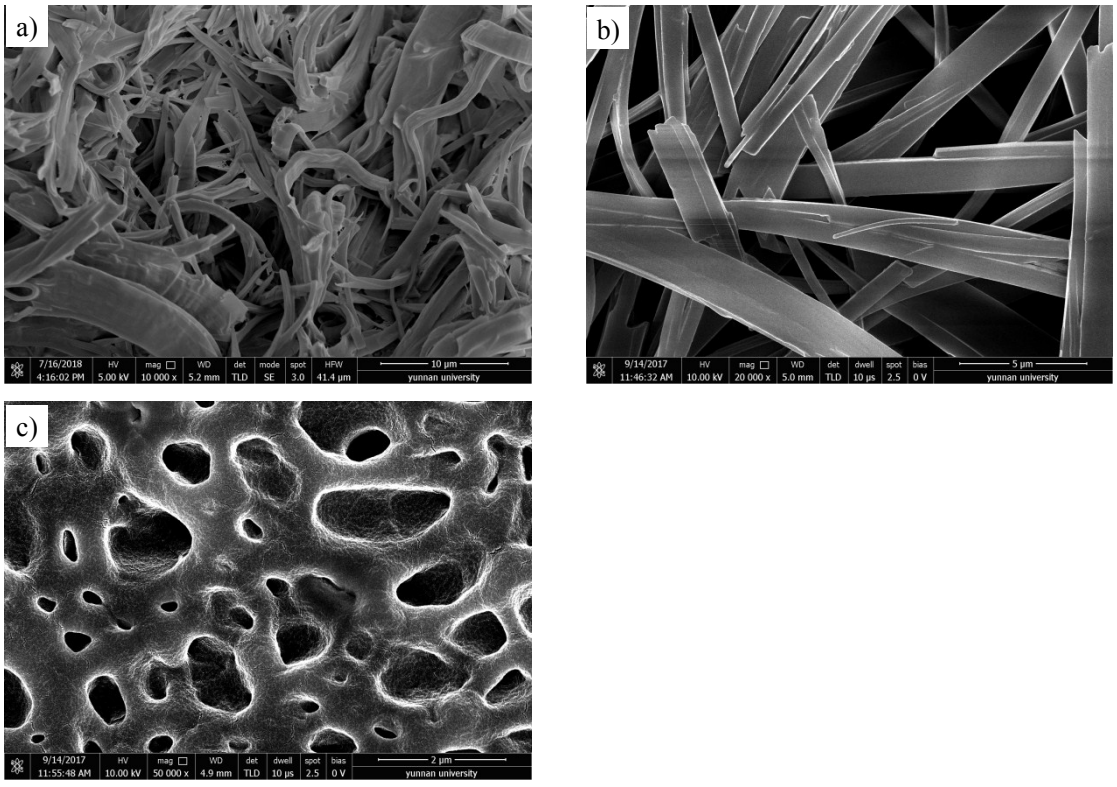

Fig. S16 (a) SEM images of xerogel of **C/10** obtained from DMF; (b) other SEM images of xerogel of **C/10** obtained from acetone; (c) other SEM images of xerogel of **C/10** obtained from *n*-hexane.

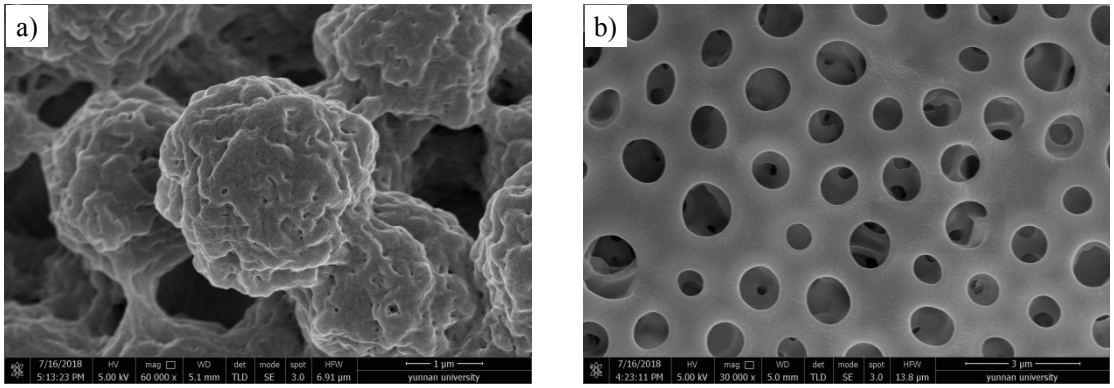

Fig. S17 Other SEM images of xerogel of **C/10** after 365 nm UV light irradiation for 2 h (a) obtained from acetone; (b) obtained from *n*-hexane.

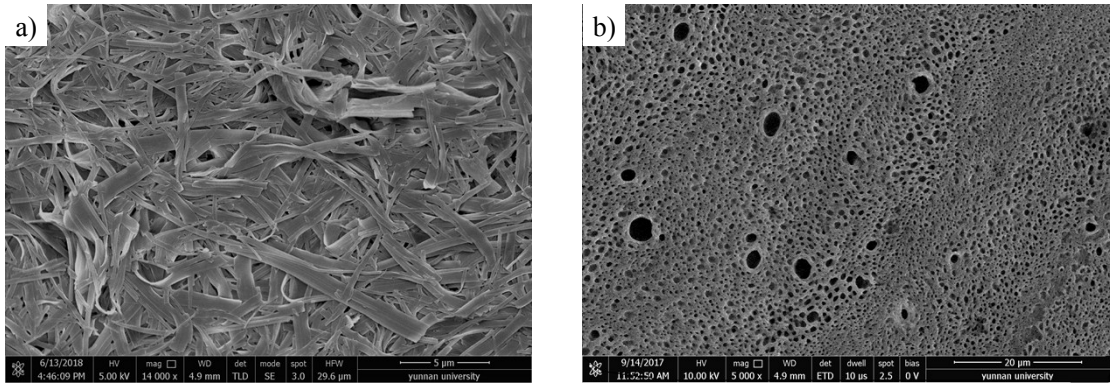

Fig. S18 SEM images of xerogel of photodimer **IC/10** after 254 nm UV light irradiation for 3 h (a) obtained from acetone; (b) obtained from *n*-hexane.

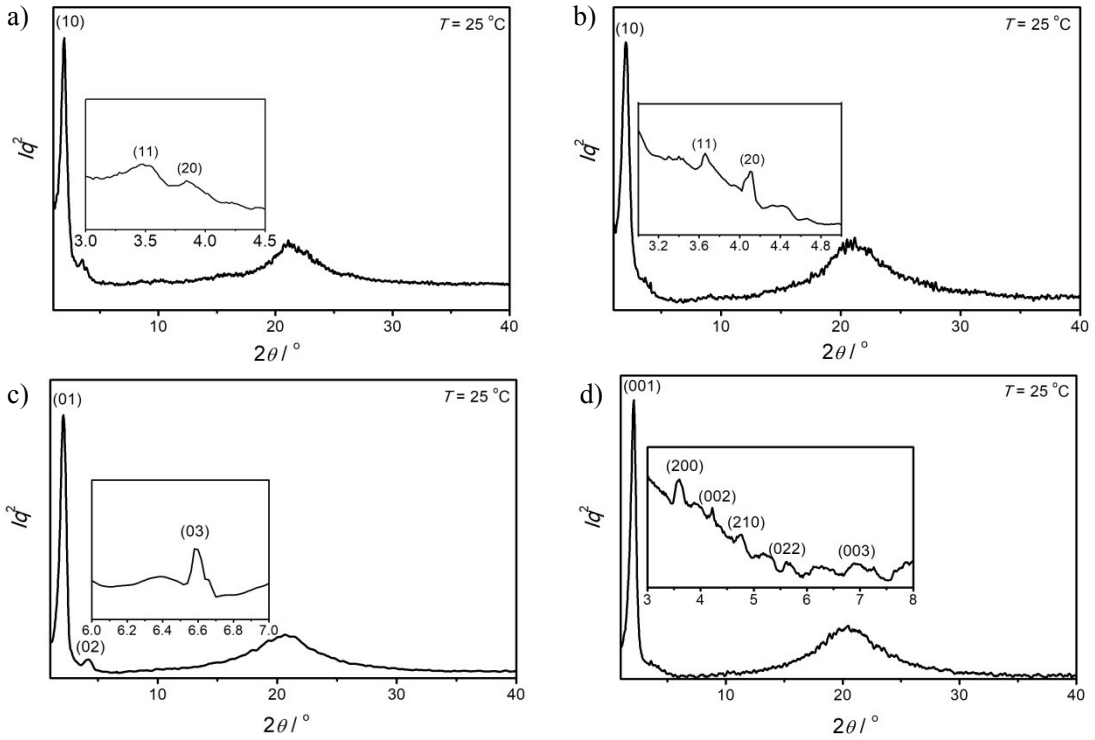

Fig. S19 (a) SAXS diffraction patterns of xerogels of **C/10** before and after 365 nm UV light irradiation (a) before irradiation in acetone; (b) after irradiation in acetone; (c) before irradiation in *n*-hexane; (d) after irradiation in *n*-hexane.

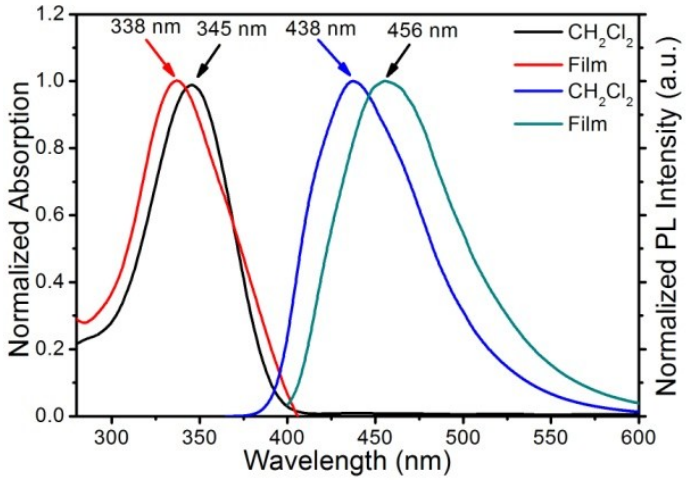

Fig. S20 Normalized absorption and emission spectra in CH_2Cl_2 solution and film for compound **C/10**.

Table S11. UV-vis absorption and fluorescence spectroscopy data of **C/10** (5×10^{-6} M) at RT.

Compd.	Solvent	λ_{ex}/nm	λ_{em}/nm	Stokes shift/nm (cm^{-1})[a]	Φ_{FL}[b]
C/10	DMF	340	430	90 (6156)	0.61
	THF	343	434	91 (6113)	0.75
	CH_2Cl_2	345	438	93 (6155)	0.79
	Hexane	348	456	108 (6806)	0.71
	Film	338	456	118 (7656)	-[c]

[a] Stokes shifts = λ_{em}–λ_{ex};

[b] Relative to quinine sulfate in 0.1 M H_2SO_4 (Φ_{FL} = 0.54) as the standard;

[c] Not measured.

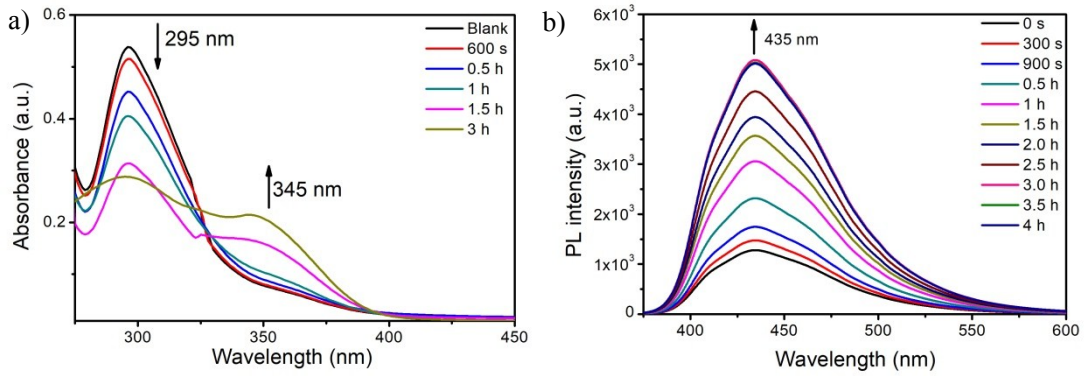

Fig. S21 (a) UV-vis spectra of photodimer **IC/10** (5×10^{-6} M) and (b) fluorescence spectra of photodimer **IC/10** (5×10^{-6} M) upon 254 nm UV light irradiation with increasing time.

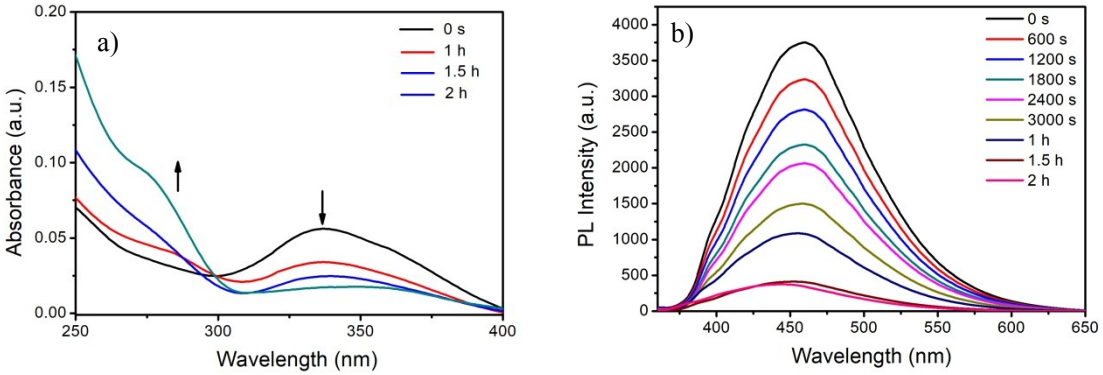

Fig. S22 (a) UV-vis spectra and (b) fluorescence spectra of compound **C/10** in film upon 365 nm UV light irradiation with increasing time.

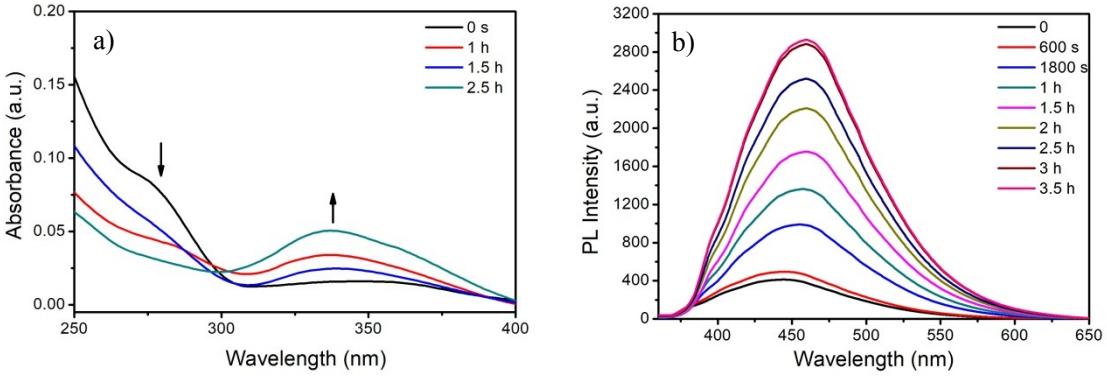

Fig. S23 (a) UV-vis spectra and (b) fluorescence spectra of photodimer **IC/10** in film upon 254 nm UV light irradiation with increasing time.

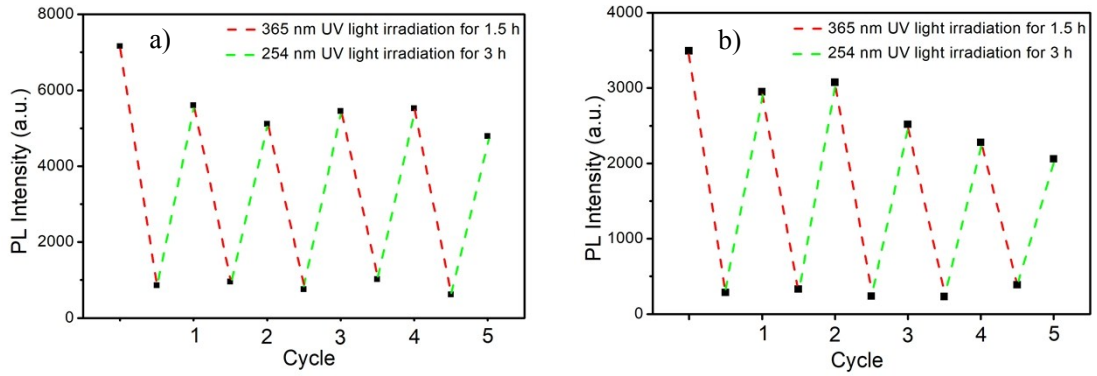

Fig. S24 Reversible changes in fluorescence intensity of **C/10** before/after irradiation with UV light (a) in CH_2Cl_2 solution; (b) in film state.

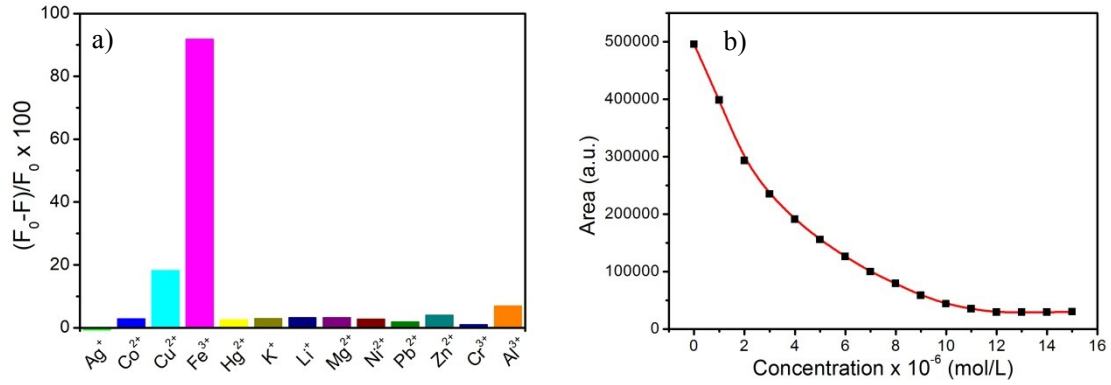

Fig. S25 (a) $(F_0\text{-}F)/F_0\times100$ depicts the metal ions selective fluorescence quenching efficiency namely the fluorescence responses of different metal ions of **C/10**; abbreviation: F_0 = the fluorescence emission maximum of the blank sample; F = the fluorescence emission maximum of samples after addition of different metal ions; (b) Fluorescence spectra of compound **C/10** (10^{-6} M) at 20 °C upon addition of Fe^{3+} (from 1 to 15.0 equiv) in in CH_2Cl_2 : CH_3CN (2:1, v/v) (λ_{ex} = 340 nm).

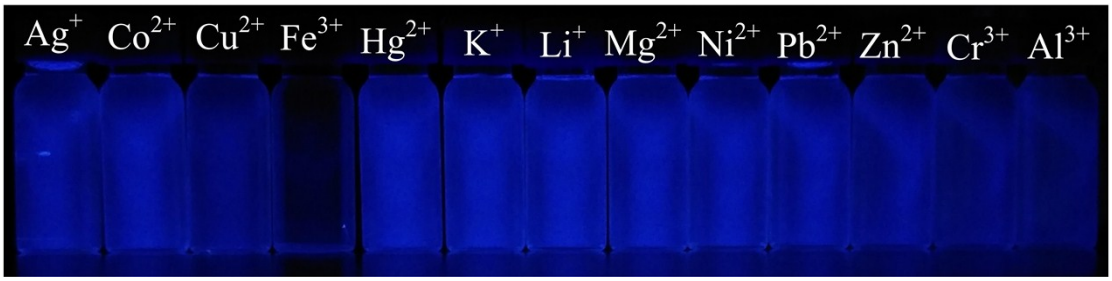

Fig. S26 Fluorescence images of compound **C/10** with addition of different metal ions, under irradiation with 365 nm light.

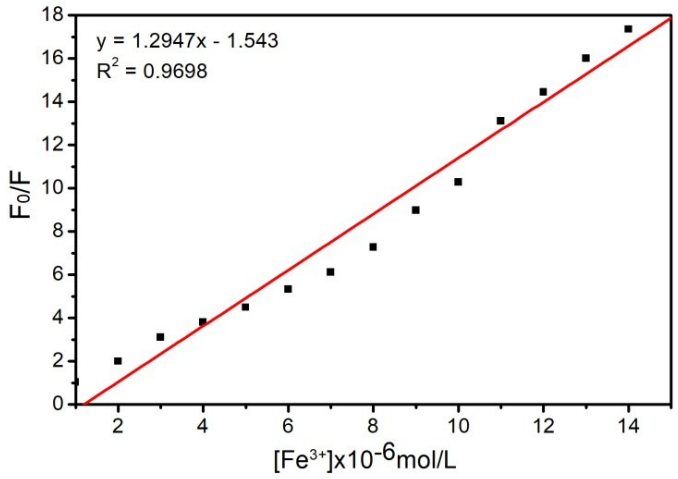

Fig. S27 Plots of the detection limits for Fe^{3+} evaluated from the fluorescence emission of **C/10**, abbreviation: F_0 = the fluorescence emission maximum of the blank sample; F = the fluorescence emission maximum of samples after addition of different metal ions.

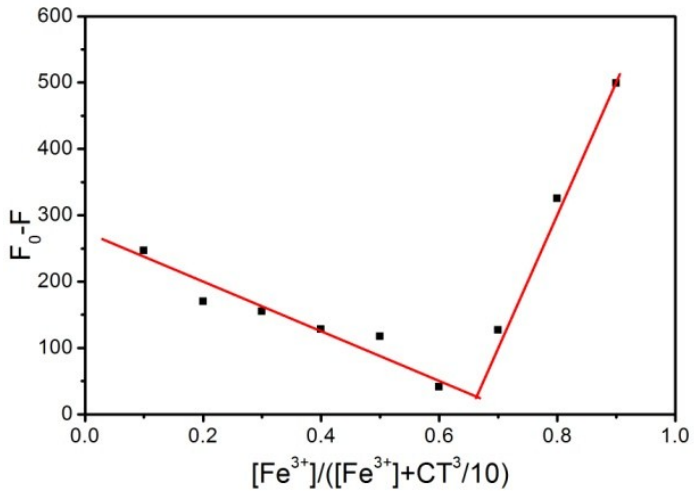

Fig. S28 Job's plots for **C/10**-Fe^{3+} in CH_2Cl_2 : CH_3CN = 2 : 1 (v/v). [**C/10**] + [Fe^{3+}] = 5.0 × 10^{-5} mol·L^{-1}, abbreviation: F_0 = the fluorescence emission maximum of the blank sample; F = the fluorescence emission maximum of samples after addition of different metal ions.

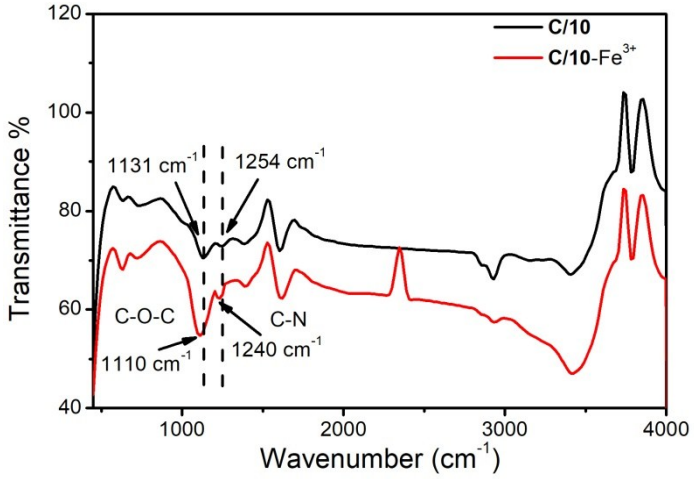

Fig. S29. FTIR spectra of (a) **C/10** and (b) **C/10**–Fe^{3+}.

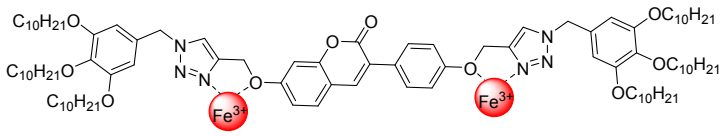

Fig. S30 The possible binding models of **C/10**–Fe^{3+}.

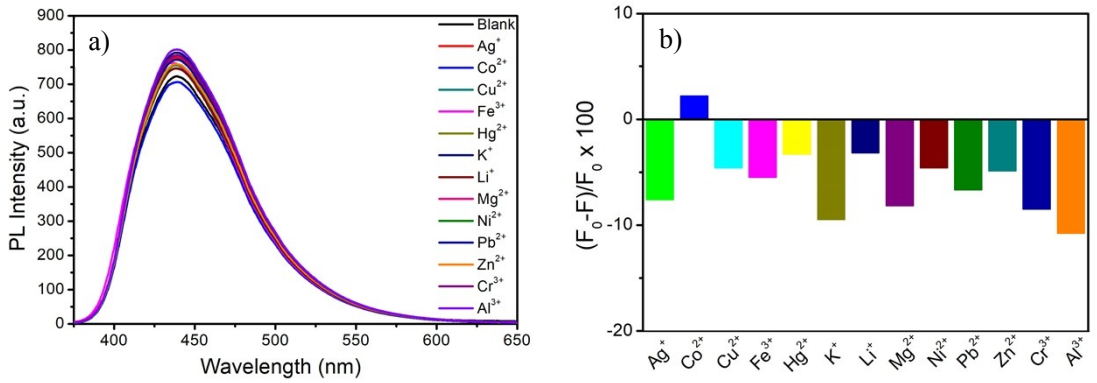

Fig. S31 (a) Fluorescence spectra of photodimer **IC/10** (10^{-6} M) with addition of metal ions (20 equiv.); (b) The metal ions selective fluorescence quenching efficiency namely the fluorescence responses of different metal ions of photodimer **IC/10**.

1.3 Materials synthesis and analytical data

For the structures of the compounds see Scheme 1 in the main text. Reactions requiring an inert gas atmosphere were conducted under argon and the glassware was oven-dried (140 °C). Tetrahydrofuran (THF) was distilled from sodium prior to use. Commercially available chemicals were used as received. ^{1}H-NMR and ^{13}C NMR spectra were recorded on a Bruker-DRX-400 spectrometer. Elemental analysis was performed using an Elementar VARIO EL elemental analyzer. Thin-layer chromatography was performed on aluminum plates precoated with 5735 silica gel 60 PF254 (Merck). Column chromatography was performed on Merck silica gel 60 (230-400 mesh).

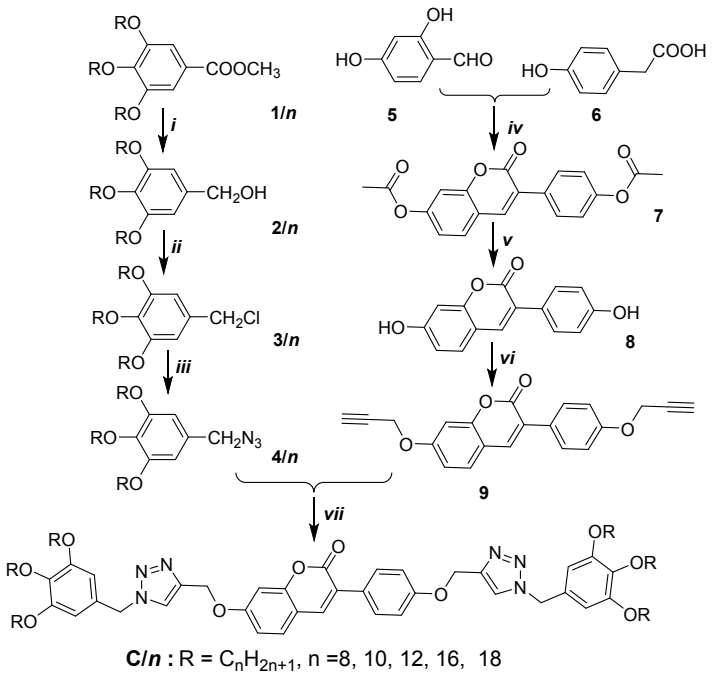

Scheme S1. Synthesis of the **C/*n***, *Reagents and conditions*: *i*) $LiAlH_4$, THF, 25 ºC, 3 h; *ii*) $SOCl_2$, THF, 25 ºC, 3 h; *iii*) NaN_3, DMF, KI, 50 ºC, 8 h; *iv*) Ac_2O, NaOAc, 190 ºC, 30 min; *v*) 3M HCl, CH_3OH, 100 ºC, 3 h; *vi*) propargyl bromide, aceton, 50 ºC, 5 h; *vii*) sodium ascorbate, $CuSO_4 \cdot 5H_2O$, tertiary butanol : H_2O = 1:1, THF, 25 ºC, 12 h.

General procedure for the synthesis of 3,4,5-tris(alkyl)benzylazide 4/*n*

Compound **4/*n*** was synthesized *via* the intermediates **1/*n***, **2/*n*** and **3/*n*** according to literature procedures in ref S2.

General procedure for the synthesis of 7[S3]

A mixture of 2,4-dihydroxybenzaldehyde (1.50 g, 0.011 mol), 2-(4-hydroxyphenyl)acetic acid (1.67 g, 0.011 mol), water-free sodium acetate (2.73 g, 0.033 mol) and acetic acid anhydride (3.59 g, 0.033 mol) were heated on an oil bath at 190 °C for 30 minutes in a round-bottomed flask. After cooling to 100°C, first water (10 ml) and then ethanol (30 ml) were added. The mixture was refluxed for additional 10 minutes. After cooling to room temperature, the solid was filtered off and washed with water and ethanol. The product was recrystallized from ethanol and THF to produce compound **7** as white solid in 87 % yield (3.23 g), m.p 199-200 °C. ^{1}H NMR (400 MHz, $CDCl_3$): δ = 7.80 (s, 1 H, Ar**H**), 7.74-7.72 (d, J = 8.8 Hz, 2 H, 2 Ar**H**), 7.56-7.54 (d, J = 8.4 Hz, 1 H, Ar**H**), 7.19-7.15 (m, 3 H, 3 Ar**H**), 7.10-7.07 (m, 1 H, Ar**H**), 2.35 (s, 3 H, OAc), 2.33 (s, 3 H, OAc).

General procedure for the synthesis of 8[S4]

Compound **7** (2.0 g, 5.91 mmol), 3M HCl (15 mL) and 60 ml methanol were refluxed with stirring at 100 °C for 3 hours. After cooling down to room temperature and removing the methanol from

the solution, the precipitate was filtered off and washed with water (3 × 20 mL). The product was recrystallized from methanol and THF.

General procedure for the synthesis of 9

Compound **8** (1.00 g, 3.93 mmol) and K_2CO_3 (1.63 g, 11.79 mmol) were added to a 50 mL round-bottomed flask. Then acetonitrile (20 mL) and propagyl bromide (1.20 g, 9.83 mmol) were added. The mixture was refluxed for 5 h. After cooling down to room temperature the acetonitrile was removed in *vacuo*. Water (50 mL) were added and the mixture was extracted with ethyl acetate (3 × 50 mL). The combined organic phases was washed with water (3 × 20 ml), dried over anhydrous Na_2SO_4 and filtrated. The solvent was evaporated in *vacuo*. The crude product was purified by a silicagel columnchromatography (dichloromethane) to produce compound **9** as white solid in 92.3% yield (1.20 g). m.p 154-156 °C. ^{1}H NMR ($CDCl_3$, 400 MHz): δ = 7.72 (s, 1 H, Ar**H**), 7.67-7.65 (d, J = 8.0 Hz, 2 H, Ar**H**), 7.46-7.44 (d, J = 8.4 Hz, 1 H, Ar**H**), 7.05-7.03 (d, J = 8.4 Hz, 2 H, Ar**H**), 6.98 (s, 1 H, Ar**H**), 6.94-6.92 (d, J = 8.8 Hz, 1 H, Ar**H**), 4.77 (s, 2 H, OC**H**$_2$), 4.73 (s, 2 H, OC**H**$_2$), 2.58 (s, 2 H, OCH$_2$C**H**), 2.54 (s, 2 H, OCH$_2$C**H**). Elemental analysis calcd (%) for $C_{21}H_{14}O_4$ (330.33); C, 76.35; H, 4.27; found: C, 76.59; H, 4.01.

General procedure for the synthesis of C/*n*

To a solution of compound **9** (33.0 mg, 0.1 mmol) and the appropriate compound **4/*n*** (0.3 mmol) in *t*-BuOH-H_2O (1 : 1, 1.5 mL) and THF (1.5 mL), $CuSO_4 \cdot 5H_2O$ (50 mg, 0.2 mmol) and sodium ascorbate (1.0 M in H_2O, 8 drops) were added. The reaction mixture was stirred at 25 °C for 24 h and the solvent was removed in *vacuo*. The residue was diluted with H_2O (5 mL) and the mixture was extracted with ethyl acetate (3 × 30 mL). The combined extracts were washed with H_2O (5 × 20 mL), anhydrous Na_2SO_4 and filtrated, then the solvent was removed in *vacuo*. The residue was purified by chromatography (dichloromethane : ethyl acetate = 20 : 1).

C/8: Yield: 102 mg, yield: 74.6%, white solid. ^{1}H NMR ($CDCl_3$, 400 MHz): δ = 7.70 (s, 1 H, Ar**H**), 7.64-7.62 (d, J = 8.8 Hz, 2 H, 2 Ar**H**), 7.58-7.55 (d, J = 12.0 Hz, 2 H, 2 Ar**H**), 7.44-7.42 (d, J = 8.4 Hz, 1 H, Ar**H**), 7.04-7.02 (d, J = 8.8 Hz, 2 H, 2 Ar**H**), 6.95 (s, 1 H, Ar**H**), 6.47 (s, 4 H, 4 Ar**H**), 5.43-5.41 (d, J = 5.6 Hz, 4 H, 2 ArC**H**$_2$Ar), 5.24-5.23 (d, J = 3.2 Hz, 4 H, 2 ArOC**H**$_2$Ar), 3.95-3.90 (m, 12 H, 6 ArOC**H**$_2$), 1.79-1.71 (m, 12 H, 6 ArOCH$_2$C**H**$_2$), 1.49-1.41 (m, 12 H, 6 ArOCH$_2$CH$_2$C**H**$_2$), 1.36-1.22 (m, 48 H, 24 C**H**$_2$), 0.90-0.86 (t, J = 6.4 Hz, 18 H, 6 C**H**$_3$). ^{13}C NMR ($CDCl_3$, 100 MHz): δ = 160.93 (1 C), 160.87 (1 C), 158.48 (1 C), 154.91 (2 C), 153.66 (2 C), 153.63 (1 C), 144.34 (1 C), 143.34 (1 C), 138.74 (1 C), 138.66 (1 C), 138.58 (1 C), 129.73 (2 C), 129.19 (1 C), 129.07 (1 C), 128.79 (1 C), 127.91 (1 C), 124.67 (1 C), 122.81 (1 C), 122.58 (1 C), 114.71 (2 C), 113.92 (1 C), 112.93 (1 C), 106.83 (2 C), 106.79 (2 C), 101.58 (1 C), 73.47 (2 C), 69.30 (2 C), 69.28 (2 C), 62.38 (1 C), 62.16 (1 C), 54.68 (1 C), 54.63 (1 C), 31.94-22.70, 14.12 (multicarbons in alkyl chains). Elemental analysis calcd (%) for $C_{83}H_{124}N_6O_{10}$ (1365.94); C, 72.89; H, 9.15; N, 6.15; found: C, 72.67; H, 9.28, N, 6.36.

C/10: Yield: 124 mg, 80.8 %, white solid. ^{1}H NMR ($CDCl_3$, 400 MHz): δ = 7.70 (s, 1 H, Ar**H**), 7.64-7.62 (d, J = 8.8 Hz, 2 H, 2 Ar**H**), 7.58-7.55 (d, J = 12.0 Hz, 2 H, 2 Ar**H**), 7.44-7.41 (d, J =

8.4 Hz, 1 H, Ar**H**), 7.04-7.02 (d, *J* = 8.8 Hz, 2 H, 2 Ar**H**), 6.95 (s, 1 H, Ar**H**), 6.47 (s, 4 H, 4 Ar**H**), 5.43-5.41 (d, *J* = 5.2 Hz, 4 H, 2 ArC**H**$_2$Ar), 5.24-5.23 (d, *J* = 2.0 Hz, 4 H, 2 ArOC**H**$_2$Ar), 3.95-3.90 (m, 12 H, 6 ArOC**H**$_2$), 3.95-3.90 (m, 12 H, 6 ArOC**H**$_2$), 1.79-1.71 (m, 12 H, 6 ArOCH$_2$C**H**$_2$), 1.46-1.41 (m, 12 H, 6 ArOCH$_2$CH$_2$C**H**$_2$), 1.38-1.25 (m, 72 H, 36 C**H**$_2$), 0.89-0.86 (t, *J* = 6.4 Hz, 18 H, 6 C**H**$_3$). ^{13}C NMR ($CDCl_3$, 100 MHz): δ = 160.93 (1 C), 160.87 (1 C), 158.48 (1 C), 154.91 (2 C), 153.66 (2 C), 153.63 (1 C), 144.33 (1 C), 143.34 (1 C), 138.74 (1 C), 138.66 (1 C), 138.58 (1 C), 129.73 (2 C), 129.20 (1 C), 129.07 (1 C), 128.79 (1 C), 127.91 (1 C), 124.67 (1 C), 122.81 (1 C), 122.58 (1 C), 114.71 (2 C), 113.92 (1 C), 112.93 (1 C), 106.83 (2 C), 106.79 (2 C), 101.58 (1 C), 73.49 (2 C), 69.30 (2 C), 69.28 (2C), 62.38 (1 C), 62.16 (1 C), 54.68 (1 C), 54.63 (1 C), 31.94-22.70, 14.12 (multicarbons in alkyl chains). Elemental analysis calcd (%) for $C_{95}H_{148}N_6O_{10}$ (1534.23); C, 74.29; H, 9.78; N, 5.45; found: C, 74.55; H, 9.61, N, 5.65.

C/12: Yield: 144 mg, 84.7 %, white solid. ^{1}H NMR ($CDCl_3$, 400 MHz): δ = 7.70 (s, 1 H, Ar**H**), 7.64-7.62 (d, *J* = 8.8 Hz, 2 H, 2 Ar**H**), 7.58-7.55 (d, *J* = 12.0 Hz, 2 H, 2 Ar**H**), 7.44-7.41 (d, *J* = 8.4 Hz, 1 H, Ar**H**), 7.04-7.02 (d, *J* = 8.8 Hz, 2 H, 2 Ar**H**), 6.95 (s, 1 H, Ar**H**), 6.48 (s, 4 H, 4 Ar**H**), 5.43-5.41 (d, *J* = 5.2 Hz, 4 H, 2 ArC**H**$_2$Ar), 5.24-5.23 (d, *J* = 2.0 Hz, 4 H, 2 ArOC**H**$_2$Ar), 3.95-3.90 (m, 12 H, 6 ArOC**H**$_2$), 3.95-3.90 (m, 12 H, 6 ArOC**H**$_2$), 1.81-1.71 (m, 12 H, 6 ArOCH$_2$C**H**$_2$), 1.46-1.43 (m, 12 H, 6 ArOCH$_2$CH$_2$C**H**$_2$), 1.40-1.28 (m, 96 H, 48 C**H**$_2$), 0.89-0.86 (t, *J* = 6.4 Hz, 18 H, 6 C**H**$_3$). ^{13}C NMR ($CDCl_3$, 100 MHz): δ = 160.92 (1 C), 160.88 (1 C), 158.49 (1 C), 154.91 (2 C), 153.67 (2 C), 153.63 (1 C), 144.33 (1 C), 143.33 (1 C), 138.73 (1 C), 138.67 (1 C), 138.59 (1 C), 129.73 (2 C), 129.20 (1 C), 129.07 (1 C), 128.78 (1 C), 127.91 (1 C), 124.68 (1 C), 122.80 (1 C), 122.56 (1 C), 114.71 (2 C), 113.92 (1 C), 112.92 (1 C), 106.83 (2 C), 106.79 (2 C), 101.58 (1 C), 73.49 (2 C), 69.28 (2 C), 69.26 (2C), 62.39 (1 C), 62.16 (1 C), 54.68 (1 C), 54.62 (1 C), 31.94-22.70, 14.12 (multicarbons in alkyl chains). Elemental analysis calcd (%) for $C_{107}H_{172}N_6O_{10}$ (1701.31); C, 75.40; H, 10.25; N, 4.90; found: C, 75.57; H, 10.08, N, 4.77.

C/16: Yield: 161 mg, 79%, white solid. ^{1}H NMR ($CDCl_3$, 400 MHz): δ = 7.70 (s, 1 H, Ar**H**), 7.64-7.62 (d, *J* = 8.8 Hz, 2 H, 2 Ar**H**), 7.58-7.55 (d, *J* = 12.0 Hz, 2 H, 2 Ar**H**), 7.44-7.41 (d, *J* = 8.4 Hz, 1 H, Ar**H**), 7.04-7.02 (d, *J* = 8.8 Hz, 2 H, 2 Ar**H**), 6.95 (s, 1 H, Ar**H**), 6.47 (s, 4 H, 4 Ar**H**), 5.43-5.41 (d, *J* = 5.2 Hz, 4 H, 2 ArC**H**$_2$Ar), 5.24-5.23 (d, *J* = 2.0 Hz, 4 H, 2 ArOC**H**$_2$Ar), 3.95-3.90 (m, 12 H, 6 ArOC**H**$_2$), 3.95-3.90 (m, 12 H, 6 ArOC**H**$_2$), 1.81-1.71 (m, 12 H, 6 ArOCH$_2$C**H**$_2$), 1.46-1.43 (m, 12 H, 6 ArOCH$_2$CH$_2$C**H**$_2$), 1.40-1.28 (m, 144 H, 72 C**H**$_2$), 0.89-0.86 (t, *J* = 6.4 Hz, 18 H, 6 C**H**$_3$). ^{13}C NMR ($CDCl_3$, 100 MHz): δ = 160.93 (1 C), 160.86 (1 C), 158.47 (1 C), 154.89 (2 C), 153.65 (2 C), 153.62 (1 C), 144.31 (1 C), 143.32 (1 C), 138.75 (1 C), 138.63 (1 C), 138.55 (1 C), 129.72 (2 C), 129.20 (1 C), 129.08 (1 C), 128.79 (1 C), 127.89 (1 C), 124.63 (1 C), 122.82 (1 C), 122.59 (1 C), 114.70 (2 C), 113.90 (1 C), 112.92 (1 C), 106.81 (2 C), 106.77 (2 C), 101.56 (1 C), 73.48 (2 C), 69.28 (2 C), 69.26 (2C), 62.36 (1 C), 62.14 (1 C), 54.66 (1 C), 54.61 (1 C), 31.93-22.68, 14.10 (multicarbons in alkyl chains). Elemental analysis calcd (%) for $C_{131}H_{220}N_6O_{10}$ (2037.69); C, 77.10; H, 11.80; N, 4.18; found: C, 77.33; H, 11.53, N, 4.37.

C/18: Yield: 191 mg, 86.5%, white solid. ^{1}H NMR ($CDCl_3$, 400 MHz): δ = 7.70 (s, 1 H, Ar**H**), 7.64-7.62 (d, *J* = 8.8 Hz, 2 H, 2 Ar**H**), 7.58-7.55 (d, *J* = 11.6 Hz, 2 H, 2 Ar**H**), 7.44-7.41 (d, *J* = 8.4 Hz, 1 H, Ar**H**), 7.04-7.02 (d, *J* = 8.8 Hz, 2 H, 2 Ar**H**), 6.95 (s, 1 H, Ar**H**), 6.47 (s, 4 H, 4 Ar**H**), 5.43-5.41 (d, *J* = 5.2 Hz, 4 H, 2 ArC**H**$_2$Ar), 5.24-5.23 (d, *J* = 2.0 Hz, 4 H, 2 ArOC**H**$_2$Ar), 3.95-

3.90 (m, 12 H, 6 ArOC**H**$_2$), 3.95-3.90 (m, 12 H, 6 ArOC**H**$_2$), 1.81-1.71 (m, 12 H, 6 ArOCH$_2$C**H**$_2$), 1.46-1.43 (m, 12 H, 6 ArOCH$_2$CH$_2$C**H**$_2$), 1.40-1.28 (m, 168 H, 84 C**H**$_2$), 0.89-0.86 (t, J = 6.4 Hz, 18 H, 6 C**H**$_3$). ^{13}C NMR ($CDCl_3$, 100 MHz): δ = 160.93 (1 C), 160.87 (1 C), 158.48 (1 C), 154.90 (2 C), 153.66 (2 C), 153.63 (1 C), 144.33 (1 C), 143.33 (1 C), 138.75 (1 C), 138.66 (1 C), 138.58 (1 C), 129.73 (2 C), 129.21 (1 C), 129.08 (1 C), 128.79 (1 C), 127.91 (1 C), 124.67 (1 C), 122.80 (1 C), 122.57 (1 C), 114.71 (2 C), 113.92 (1 C), 112.92 (1 C), 106.83 (2 C), 106.79 (2 C), 101.58 (1 C), 73.48 (2 C), 69.30 (2 C), 69.27 (2C), 62.39 (1 C), 62.16 (1 C), 54.67 (1 C), 54.62 (1 C), 31.94-22.68, 14.11 (multicarbons in alkyl chains). Elemental analysis calcd (%) for $C_{143}H_{244}N_6O_{10}$ (2205.88); C, 77.89; H, 11.10; N, 3.76; found: C, 77.67; H, 10.98, N, 3.56.

References

[S1] Z. Li, Z. Wu, G. Mo, X. Xing, P. Liu, *Instrum. Sci. Technol.*, 2014, **42**, 128−141.

[S2] (a) X. P. Tan, L. Y. Kong, H. Dai, X. H. Cheng, F. Liu and C. Tschierske, *Chem. Eur. J.*, 2013, **19**, 16303–16313; (b) M. Lammens, J. Skey, S. Wallyn, R. O'Reilly and F. D. Prez, *Chem. Commun.*, 2010, **46**, 8719–8721; (c) D. X. Huang, M. Prehm, H. F. Gao, X. H. Cheng, Y. S. Liu, C. Tschierske, *RSC Adv.*, 2016, **6**, 21387–21395.

[S3] (a) L. M. Kabeya, A. A. de Marchi, A. Kanashiro, N. P. Lopes, C. H. T. P. da Silva, M. T. Pupob, and Y. M. Lucisano-Valima, *Bioorg. Med. Chem.*, 2007, **15**, 1516–1524; (b) A. Fais, M, Corda, B. Era, M. B. Fadda, M. J. Matos, E. Quezada, L. Santana, C. Picciau, G. Podda, G. Delogu, *Molecules.,* 2009*,* **14**, 2514–2520.

[S4] X. H. Huang, J. Liu, J. F. Sheng, X. H. Song, Z. B. Du, M. K. Li, X. J. Zhang and Y. Zou, *Green Chem.*, 2018, **20**, 804–808.